Left-handed electromagnetic waves in materials with induced polarization and magnetization

D. D. Yavuz and N. R. Brewer
Department of Physics, 1150 University Avenue, University of Wisconsin at Madison, Madison, Wisconsin, 53706, USA
(Received 27 June 2014; revised manuscript received 30 October 2014; published 5 December 2014)

We analyze the properties of electromagnetic waves inside materials with induced polarization and magnetization. We show that if the polarization and magnetization of the material are sufficiently large and appropriately phased, then the system supports the formation of left-handed waves. In some respects, such a system behaves similarly to materials with a negative index of refraction, yet there is one important advantage: Left-handed waves in materials with induced polarization and magnetization do not require as stringent material properties (such as the strength of resonances and the density of radiators). We numerically investigate the formation and propagation of such left-handed waves using finite-difference approximation to Maxwell's equations. We also discuss possible experimental observation of these ideas in a rare-earth-doped crystal.

DOI: 10.1103/PhysRevA.90.063807 PACS number(s): 42.70.−a, 78.20.Ci, 42.65.An, 81.05.Xj

I. INTRODUCTION

Over the past decade, the interest in left-handed electromagnetic waves where E, H, and k vectors form a left-handed triad has been continuously growing. The most well-known example of materials that support left-handed waves are negative-index materials. These materials were first predicted by Veselago, who argued that materials with a simultaneously negative permittivity and permeability would exhibit a negative refractive index (throughout this paper the term *negative refractive index* is reserved for materials in the sense exactly described by Veselago) [1]. Although the interest in negative index remained a scientific curiosity for a long time, it is now understood that these materials may have important applications such as constructing lenses that beat the diffraction limit [2–4] and engineering electromagnetic cloaks [5,6]. Two different (and somewhat complementary) approaches are currently being pursued to construct negative-index materials: (i) metamaterials [7–16] and (ii) atomic systems [17–23]. Negative refraction has so far been experimentally demonstrated in both the microwave [7–10] and the optical [11–16] regions of the spectrum, with all experiments thus far relying on metamaterials. The second approach uses sharp electric-dipole and magnetic-dipole transitions of atoms to modify the permittivity and permeability appropriately to achieve a negative refractive index. In the spirit of electromagnetically induced transparency (EIT) and related techniques [24,25], the idea is to dress the atomic system with strong lasers in such a way to produce a negative refractive index for a weak probe beam.

Constructing negative-index materials has so far been challenging due to a number of difficulties: (i) The permittivity and permeability have to be simultaneously modified, and as a result, one needs both electric and magnetic resonances near the same wavelength. (ii) The electric and magnetic resonances of the system have to be strong, which translates into stringent requirements on the number of radiators required. In atomic systems, all suggested schemes require atomic densities in excess of 10^{16} atoms/cm^3 [17–23]. In many experimental systems it is simply not possible to achieve such high densities and simultaneously preserve sharp atomic transitions (linewidths at the level of 1 MHz are required). (iii) An ensemble of radiators that satisfies these first two requirements typically produces large absorption [26]. This is particularly pronounced in the optical domain where the imaginary part of the refractive index is typically almost as large as the real part. This is a key limitation for many potential applications since light is largely absorbed within a few wavelengths of propagation inside the material. There has been some recent progress on overcoming absorption using active metamaterials [27]. In atomic systems, absorption can, in principle, be overcome using quantum interference ideas such as EIT or the interference of two Raman transitions [19,21]. Nevertheless, these difficulties that are outlined in this paragraph are formidable for many experimental implementations of negative index. Due to these difficulties, negative index in atomic systems has not yet been experimentally observed. Furthermore, although there have been many exciting experimental results from the metamaterial community, the performances of the constructed negative-index materials are still far from what is needed for practical applications. For example, it is still not clear if it will be possible to construct widely applicable super-resolution optical microscopes using negative-index materials.

We therefore feel strongly that it is important to investigate alternative ideas that exhibit some of the physics and applications of negative-refractive-index materials. In this paper, we study the propagation of electromagnetic waves inside a material where the medium is polarized and magnetized externally (i.e., through means other than the incident electromagnetic wave). We argue that if the induced polarization and magnetization are sufficiently large and appropriately phased, then the medium will support the formation of left-handed waves. Such materials appear to manifest much of the physics of negative-index materials. Compared to materials with a negative refractive index, there is one clear advantage of materials with induced polarization and magnetization: The formation of left-handed waves does not require the stringent material properties (such as the strength of the resonances, the density of radiators, and so on). As a result, the ideas presented in this paper may result in (1) an observation of left-handed waves in atomic systems and (2) more practical and flexible metamaterials for left-handed wave studies.

II. FORMALISM AND ANALYTICAL RESULTS

We begin our discussion by rewriting Maxwell's equations inside a polarized and magnetized

material:

$$\begin{aligned} \nabla \times \vec{\mathcal{E}} &= -\frac{\partial \vec{\mathcal{B}}}{\partial t}, \\ \nabla \times \vec{\mathcal{H}} &= \frac{\partial \vec{\mathcal{D}}}{\partial t}, \\ \nabla \cdot \vec{\mathcal{D}} &= 0, \\ \nabla \cdot \vec{\mathcal{B}} &= 0, \end{aligned} \tag{1}$$

where the displacement vector $\vec{\mathcal{D}}$ and the magnetic field $\vec{\mathcal{B}}$ are modified inside a material to include the polarization ($\vec{\mathcal{P}}$) and the magnetization ($\vec{\mathcal{M}}$):

$$\begin{aligned} \vec{\mathcal{D}} &= \epsilon_0 \vec{\mathcal{E}} + \vec{\mathcal{P}}, \\ \vec{\mathcal{B}} &= \mu_0 \vec{\mathcal{H}} + \mu_0 \vec{\mathcal{M}}. \end{aligned} \tag{2}$$

The medium can be polarized and magnetized at a specific frequency ω using a number of processes. The most obvious one would be if the frequency of the incident electromagnetic wave is close to an electric-dipole (or a magnetic-dipole) resonance, then the incident wave itself can polarize (or magnetize) the medium through the linear response of the material. Physically, macroscopic polarization can be visualized as an ensemble of microscopic electric dipoles oscillating in unison. Similarly, macroscopic magnetization can be visualized as an ensemble of magnetic dipoles (current loops) oriented along a common direction. It is important to note that the medium can also be polarized or magnetized at a frequency ω using external means (i.e., processes that do not depend on the incident electromagnetic wave). Throughout this paper, we focus on externally induced polarization and magnetization. This can be accomplished, for example, by applying powerful lasers at other frequencies and using the nonlinear response of the material. We discuss a specific scheme later in this paper.

Using Eq. (2), the first two of the Maxwell's equations inside a material can be reduced to

$$\begin{aligned} \nabla \times \vec{\mathcal{E}} &= -\mu_0 \frac{\partial \vec{\mathcal{H}}}{\partial t} - \mu_0 \frac{\partial \vec{\mathcal{M}}}{\partial t}, \\ \nabla \times \vec{\mathcal{H}} &= \epsilon_0 \frac{\partial \vec{\mathcal{E}}}{\partial t} + \frac{\partial \vec{\mathcal{P}}}{\partial t}. \end{aligned} \tag{3}$$

We now look for plane wave solutions of Eq. (3). We assume that the medium is polarized and magnetized at the same frequency ω with exactly the same k vector and take $\vec{\mathcal{P}} = \vec{P}\exp(i\vec{k}\cdot\vec{r} - i\omega t)$ and $\vec{\mathcal{M}} = \vec{M}\exp(i\vec{k}\cdot\vec{r} - i\omega t)$. With the assumed polarization and magnetization, we look for forced-wave solutions for the fields, $\vec{\mathcal{E}} = \vec{E}\exp(i\vec{k}\cdot\vec{r} - i\omega t)$ and $\vec{\mathcal{H}} = \vec{H}\exp(i\vec{k}\cdot\vec{r} - i\omega t)$. With plane waves, Maxwell's equations reduce to

$$\begin{aligned} \vec{k} \times \vec{E} &= \mu_0 \omega (\vec{H} + \vec{M}), \\ \vec{k} \times \vec{H} &= -\omega (\epsilon_0 \vec{E} + \vec{P}). \end{aligned} \tag{4}$$

From Eq. (4), we see that if the $\vec{E}$ and $\vec{H}$ vectors are chosen to be of appropriate magnitude and π out of phase with the induced polarization and magnetization, there would be sign flips on the right-hand side of the equations. A particularly interesting case, which we focus on in the remainder of this paper, is if the field quantities are chosen such that

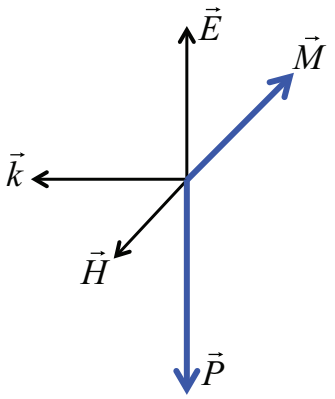

FIG. 1. (Color online) Left-handed waves inside a material with induced polarization and magnetization. If the medium is polarized and magnetized at the same frequency ω with exactly the same k vector, then there are forced-wave solutions with the vectors $\vec{E}$, $\vec{H}$, and $\vec{k}$ forming a left-handed triad. The solutions are such that the field quantities $\vec{E}$ and $\vec{H}$ are π out of phase with the induced polarization and magnetization.

$\vec{H} = -\vec{M}/2$ (or equivalently $\vec{M} = -2\vec{H}$), and $\vec{E} = -\vec{P}/2\epsilon_0$ ($\vec{P} = -2\epsilon_0\vec{E}$), which results in

$$\begin{aligned} \vec{k} \times \vec{E} &= -\mu_0 \omega \vec{H}, \\ \vec{k} \times \vec{H} &= \epsilon_0 \omega \vec{E}. \end{aligned} \tag{5}$$

The relations given in Eq. (5) are identical to the ones in free space, except for a sign change on the right-hand side of the equations. We note that this sign change can also be thought of as flipping the signs of permittivity and permeability; i.e., we would have obtained Eq. (5) if we had started with Maxwell's equations in free space and had made the substitution $\mu_0 \to -\mu_0$ and $\epsilon_0 \to -\epsilon_0$ (as is the case for $n = -1$). Equation (5) indicates that the vectors $\vec{E}$, $\vec{H}$, and $\vec{k}$ now form a left-handed triad. This is shown in Fig. 1. Furthermore, using the product of the two equations, it can be seen that the dispersion relation is identical to that of free space: $k = \omega/c$ ($k \equiv |\vec{k}|$, c: speed of light in vacuum). It is remarkable that, under these conditions, the wave propagates without absorption or gain even though the medium is highly polarized and magnetized. The consistency of the solutions requires a particular relationship between the magnitudes of the induced polarization and magnetization: $|\vec{M}| = c|\vec{P}|$. Inspecting Eq. (5), as the frequency of the wave increases, the direction of the k vector remains unchanged (i.e., the wave remains left-handed) while its magnitude increases. As a result, the group velocity of the wave, $d\omega/dk$, is parallel to the k vector. This is in contrast to negative-index materials where the phase and group velocities are antiparallel. It therefore appears that the analogy with negative-index materials should not be carried too far. Although there are many similarities between materials with induced polarization and magnetization and negative-index materials, there are also major differences. We discuss one similarity below, where we numerically show negative refraction at an interface. It is important to note that the above analytical treatment is valid for a single-spatial mode of light (i.e., for only a single k vector). As we discuss below, our numerical results show that these ideas remain valid even

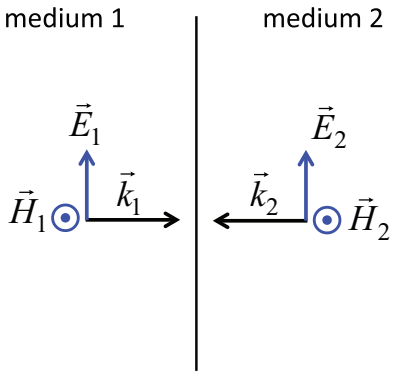

FIG. 2. (Color online) Beam refraction at normal incidence from a right-handed material into a material with induced polarization and magnetization. The boundary conditions at the interface dictate that $\vec{E}_2 = \vec{E}_1$ and $\vec{H}_2 = \vec{H}_1$. If the induced polarization and magnetization in medium 2 are $\vec{M} = -2\vec{H}_2$ and $\vec{P} = -2\epsilon_0\vec{E}_2$, then forced left-handed waves are excited. These waves satisfy both the boundary conditions at the interface and Maxwell's equations in the material.

for spatial wave packets, i.e., when there are many k vectors simultaneously present.

We next discuss how to excite these forced waves inside the material by considering refraction at an interface at normal incidence. Consider an electromagnetic wave refracting from a "normal," right-handed material (medium 1) to a material with induced polarization and magnetization (medium 2) as shown in Fig. 2. For simplicity, we take medium 1 to be free space, though the arguments hold for any right-handed material. The boundary conditions at the interface state that the tangential components of the E and H fields must be continuous at the interface. For the geometry of Fig. 2, we must have $\vec{E}_2 = \vec{E}_1$ and $\vec{H}_2 = \vec{H}_1$. We assume that in medium 2, we are able to prepare appropriately phased polarization and magnetization with $\vec{M} = -2\vec{H}_2$ and $\vec{P} = -2\epsilon_0\vec{E}_2$ (imitating a material with $n = -1$). The refraction problem is particularly simplified for this case since the two materials are impedance matched and there is no reflected wave. Under these conditions, the forced left-handed waves of Eq. (5) satisfy both the boundary conditions at the interface and the Maxwell's equations in the material.

III. SPECIFIC IMPLEMENTATION USING SECOND-ORDER NONLINEARITY

For concreteness, we next focus on a specific scheme for the implementation of these ideas in a model atomic system. We discuss possible experimental implementation in a rare-earth-doped crystal later in the paper. As shown in Fig. 3, to polarize and magnetize the medium, we utilize second-order nonlinearity ($\chi^{(2)}$) using three intense laser beams with fields E_a, E_b (electric field), and B_c (magnetic field). The energy level diagram of Fig. 3 can be realized experimentally using, for example, laser-cooled rare-earth atomic clouds or rare-earth-doped crystals [22]. The beams two-photon excite an electric-dipole ($|g\rangle \rightarrow |e\rangle$) and a magnetic-dipole ($|g\rangle \rightarrow |m\rangle$) transition through an intermediate level $|r\rangle$. The states $|g\rangle$ and $|m\rangle$ have the same parity, which is opposite to the parity of states $|r\rangle$ and $|e\rangle$. To simplify the problem, we focus on the

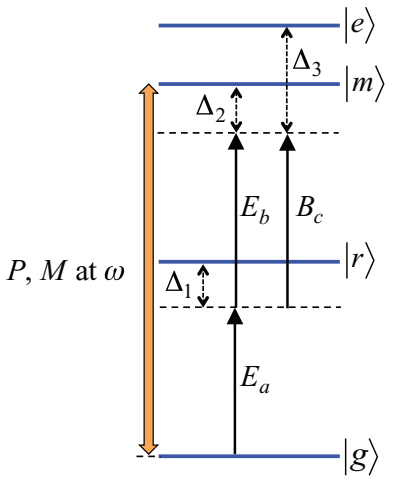

FIG. 3. (Color online) Inducing polarization and magnetization using second-order atomic nonlinearity $\chi^{(2)}$. Three intense laser beams with fields E_a, E_b (electric), and B_c (magnetic), two-photon excite an electric-dipole ($|g\rangle \rightarrow |e\rangle$) and a magnetic-dipole ($|g\rangle \rightarrow |m\rangle$) transition through an intermediate level $|r\rangle$. The nonlinear response produces polarization and magnetization at the sum frequency of $\omega = \omega_a + \omega_b = \omega_a + \omega_c$.

second-order response of Fig. 3 and ignore other nonlinear processes. The polarization and magnetization induced in the medium are

$$\begin{aligned} P &= N d_{ge}\rho_{ge}, \\ M &= N\mu_{gm}\rho_{gm}. \end{aligned} \tag{6}$$

Here N is the density of radiators, and we have defined $P \equiv |\vec{P}|$ and $M \equiv |\vec{M}|$. The quantities d_{ge} and μ_{gm} are the electric and magnetic dipole matrix elements between respective states. ρ_{ge} and ρ_{gm} are the coherences, and within the perturbative limit they are given by

$$\begin{aligned} \rho_{gm} &= \frac{\Omega_a\Omega_b}{4(\Delta_1 + i\Gamma_r/2)(\Delta_2 + i\Gamma_m/2)}, \\ \rho_{ge} &= \frac{\Omega_a\Omega_c}{4(\Delta_1 + i\Gamma_r/2)(\Delta_3 + i\Gamma_e/2)}. \end{aligned} \tag{7}$$

In Eq. (7), the quantities $\Omega_a = E_a d_{gr}/\hbar$, $\Omega_b = E_b d_{rm}/\hbar$, and $\Omega_c = B_c\mu_{re}/\hbar$ are the Rabi frequencies of the applied fields. The detunings from respective levels are defined as $\Delta_1 = (\omega_r - \omega_g) - \omega_a$, $\Delta_2 = (\omega_m - \omega_g) - (\omega_a + \omega_b)$, and $\Delta_3 = (\omega_e - \omega_g) - (\omega_a + \omega_c)$. Γ_r, Γ_e, and Γ_m are the decay rates of the respective levels. The microscopic coherences calculated using Eq. (7) produce the macroscopic polarization and magnetization at the sum frequency of $\omega = \omega_a + \omega_b = \omega_a + \omega_c$. The induced polarization and magnetization then interact with the electric and magnetic field components (E and H) of the probe wave to produce left-handed waves under appropriate conditions. We note, once again, the essential difference of our approach compared to negative-index materials. In negative-index materials, the medium would be polarized and magnetized by the probe wave itself. This essentially means that the coherences of the magnetic-dipole and electric-dipole transitions would be proportional to the electric and magnetic field components of the probe wave. In

contrast, in our approach, the coherences of Eq. (7) are induced externally with additional laser beams.

IV. LEFT-HANDED WAVE INTENSITY

A key advantage of the proposal of this paper is that these effects can be observed at low atomic densities. There is not a strict density threshold as there is for constructing negative-index materials. Rather, the density of radiators limits the magnitudes of the induced polarization and magnetization, which in turn limit the E and H fields (and therefore the intensity) of the left-handed waves. Figure 4 shows the calculated relationship between atomic density and left-handed wave generation. In these calculations, we consider a model atomic system with electric and magnetic dipole matrix elements $d_{ge} = ea_0$ (e is electron charge, a_0 is Bohr radius) and $\mu_{gm} = \mu_B$ (μ_B is Bohr magneton). We also assume the ideal case of maximum coherence for the respective transitions; i.e., $\rho_{ge} \approx \rho_{gm} \approx 1/2$. Such high coherences would require Rabi frequencies for the fields of order the detunings from the respective transitions, $\Omega \sim \Delta$. Under these conditions, for a given atomic density N, we calculate the maximum possible polarization and magnetization that can be achieved in the material [Eq. (6)], which in turn determines the field values for the left-handed waves (using $|\vec{H}| = |\vec{M}|/2$ and $|\vec{E}| = |\vec{P}|/2\epsilon_0$). We find that the maximum possible magnetization of the material places a more stringent requirement on the intensity of the waves than that of the polarization. This is similar to the problem of constructing negative-index materials where the strength of the magnetic interaction is typically the chief difficulty. In Fig. 4, we plot the intensity of the left-handed waves that can be formed as the atomic density is varied. We find that even at atomic densities as low as $10^{12}/\text{cm}^3$, left-handed waves can be formed with intensities that can be measured with state-of-the-art detection techniques. In contrast, all negative-index proposals in atomic systems require densities exceeding $10^{16}/\text{cm}^3$ [17–23]. As a result, our proposal may be the only practical proposal with the possibility to observe left-handed waves in atomic systems.

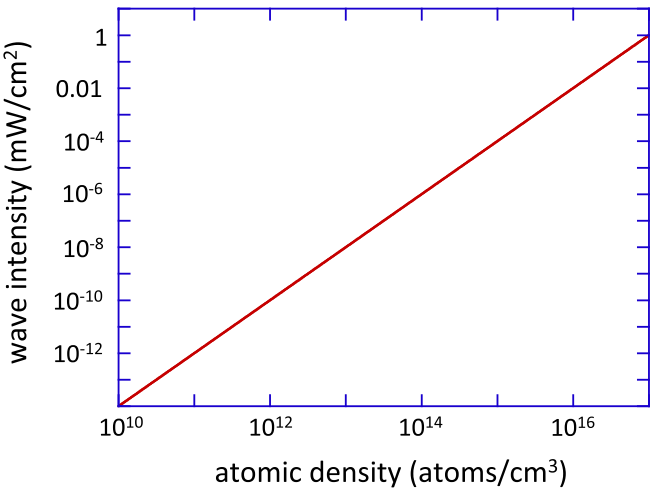

FIG. 4. (Color online) The calculated intensity of the left-handed waves that can be formed as the atomic density is varied. For atomic densities of $10^{12}/\text{cm}^3$ (which is achievable with most vapor cells or laser-cooled ultracold clouds), left-handed waves with intensities of about 1 pW/cm^2 can be formed. In contrast, all negative-index proposals in atomic systems require densities exceeding $10^{16}/\text{cm}^3$.

V. NUMERICAL SIMULATIONS

We proceed with a discussion of the numerical simulations [28]. To facilitate the simulations, we consider TE waves in two spatial dimensions x and y with electric and magnetic field components $\vec{\mathcal{E}} = \hat{z}\mathcal{E}_z(x,y,t)$ and $\vec{\mathcal{H}} = \hat{x}\mathcal{H}_x(x,y,t) + \hat{y}\mathcal{H}_y(x,y,t)$. The corresponding polarization and magnetization components are $\vec{\mathcal{P}} = \hat{z}\mathcal{P}_z(x,y,t)$ and $\vec{\mathcal{M}} = \hat{x}\mathcal{M}_x(x,y,t) + \hat{y}\mathcal{M}_y(x,y,t)$. With these components, Maxwell's equations written in a form most suitable for the finite-difference technique are

$$\begin{aligned}
\frac{\partial \mathcal{E}_z}{\partial t} &= \frac{1}{\epsilon_0}\left(\frac{\partial \mathcal{H}_y}{\partial x} - \frac{\partial \mathcal{H}_x}{\partial y}\right) - \frac{1}{\epsilon_0}\frac{\partial \mathcal{P}_z}{\partial t}, \\
\frac{\partial \mathcal{H}_x}{\partial t} &= -\frac{1}{\mu_0}\frac{\partial \mathcal{E}_z}{\partial y} - \frac{\partial \mathcal{M}_x}{\partial t}, \\
\frac{\partial \mathcal{H}_y}{\partial t} &= \frac{1}{\mu_0}\frac{\partial \mathcal{E}_z}{\partial x} - \frac{\partial \mathcal{M}_y}{\partial t}.
\end{aligned} \tag{8}$$

We take the polarization and magnetization to be known functions of space and time (externally induced) and numerically integrate Eqs. (8) to find the electric and magnetic field components at all time points. We perform the numerical integration in a three-dimensional spatiotemporal grid with grid spacings of Δx, Δy, and Δt. To assure numerical stability, we choose $\Delta t << \Delta x/c, \Delta y/c$. We start the integration with the specified initial conditions $\mathcal{E}_z(x,y,t=0)$, $\mathcal{H}_x(x,y,t=0)$, and $\mathcal{H}_y(x,y,t=0)$, and use the fourth-order Runge-Kutta algorithm to advance the field quantities in time.

Figure 5 shows pure left-handed wave propagation through a polarized and magnetized material. Here, we assume externally induced polarization and magnetization waves propagating along $+x$ direction with the functional forms:

$$\begin{aligned}
\mathcal{P}_z &= P_{z0}\cos\left[k(x-ct)\right]\exp\left[-(x-ct)^2/W_x^2\right], \\
\mathcal{M}_y &= M_{y0}\cos\left[k(x-ct)\right]\exp\left[-(x-ct)^2/W_x^2\right],
\end{aligned} \tag{9}$$

and $\mathcal{M}_x = 0$. As mentioned above, in Eq. (9), the quantities P_{z0} and M_{y0} are related through the speed of light, $M_{y0} = cP_{z0}$. We take the wavelength to be $\lambda = 2\pi/k = 1\ \mu$m. The quantity W_x determines the width of the wave packet and is chosen to be $W_x = 7\ \mu$m. For the numerical simulation of Fig. 5, we choose the initial conditions for the field values to be the ideal case as required for left-handed wave excitation $\mathcal{E}_z(x,y,t=0) = -\mathcal{P}_z(x,y,t=0)/2\epsilon_0$ and $\mathcal{H}_y(x,y,t=0) = -\mathcal{M}_y(x,y,t=0)/2$. Figure 5 shows the snapshots for the electric field $\mathcal{E}_z$ along the x coordinate at $t = 0$, $t = 1$, and $t = 60$ fs. The two plots at $t = 0$ and $t = 1$ fs clearly show that the phase velocity and therefore the k vector is oriented along the $+x$ direction (for visual aid, the dashed vertical line is aligned to $t = 0$). This is a left-handed wave since the electric and magnetic field components are oriented along $+z$ and $+y$ directions, respectively. Furthermore, the group velocity of the wave is also oriented along the $+x$ direction. As expected from the analytical solution discussed above, the wave propagates without any absorption or gain and at the speed c.

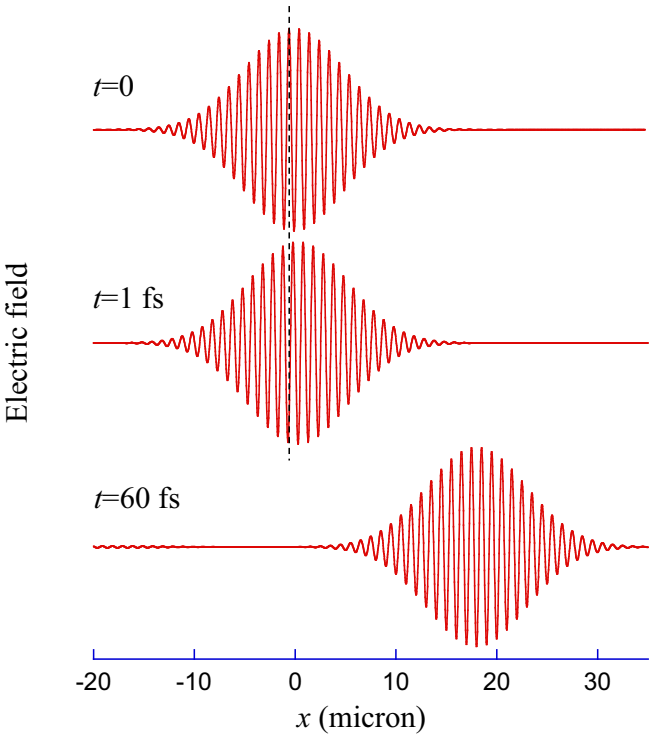

FIG. 5. (Color online) Finite-difference numerical simulations of Maxwell's equations that demonstrate left-handed waves inside a material with induced polarization and magnetization. The plots show the snapshots for the electric field of a wave packet at three different instants in time, $t = 0$, $t = 1$, and $t = 60$ fs. Both the phase and group velocities are oriented along the $+x$ direction. The electric and magnetic field components are oriented along $+z$ and $+y$ directions, respectively.

Figure 6 shows the results of numerical simulations where the initial field values are chosen to be $\mathcal{E}_z(x,y,t=0) = \mathcal{H}_y(x,y,t=0) = 0$. Other parameters are identical to those of the numerical simulation of Fig. 5. The plots in Fig. 6 show the snapshots for the electric field $\mathcal{E}_z$ at $t = 0$, $t = 1$, $t = 30$, and $t = 60$ fs, respectively. In addition to a left-handed wave, a right-handed wave of appropriate amplitude is formed. This result can be understood as follows. From superposition principle, we may add any homogeneous solution to Maxwell's equations to the left-handed wave solutions. Homogeneous solutions are the solutions without any driving terms, i.e., without any externally induced polarization and magnetization (right-handed waves). If the initial conditions for the fields are different from those required for pure left-handed wave excitation [$\mathcal{E}_z(x,y,t=0) = -\mathcal{P}_z(x,y,t=0)/2\epsilon_0$ and $\mathcal{H}_y(x,y,t=0) = -\mathcal{M}_y(x,y,t=0)/2$], then we may add an appropriate right-handed wave solution such that the initial condition is satisfied. For zero-field initial condition, as is the case in the numerical simulation of Fig. 6, the right-handed component has an equal magnitude and opposite phase such that there is perfect destructive interference with the left-handed wave at $t = 0$.

We next present a more detailed analysis of refraction at an interface. Similar to the discussion of Fig. 2, consider an electromagnetic wave refracting from free space to a material with induced polarization and magnetization (medium 2)

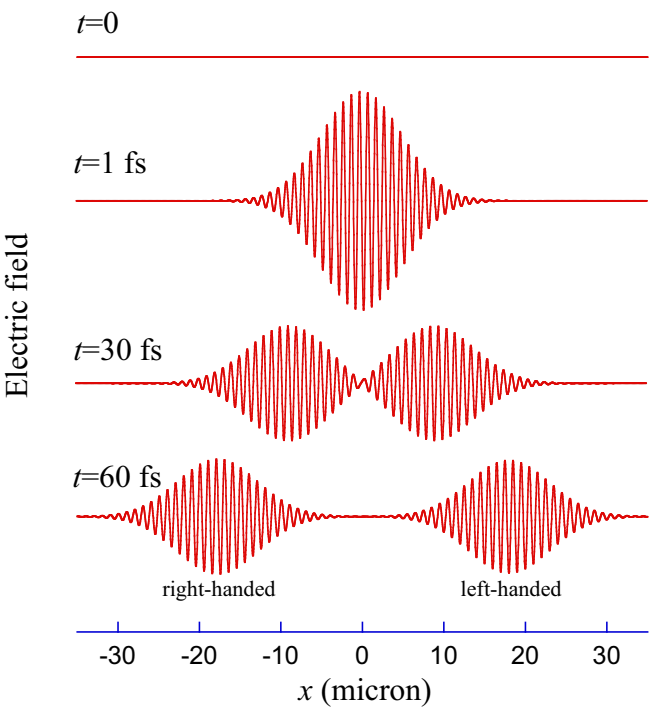

FIG. 6. (Color online) Wave propagation with the initial field values chosen to be $\mathcal{E}_z(x,y,t=0) = \mathcal{H}_y(x,y,t=0) = 0$. In addition to a left-handed wave, a right-handed wave with equal amplitude and opposite initial phase (phase at $t = 0$) is formed.

but now with an arbitrary angle as shown in Fig. 7(a). The boundary conditions at the interface state that (i) the tangential components of E and H must be continuous at the boundary and (ii) the normal components of B and D must be continuous at the boundary. We assume that in medium 2 we are able to prepare appropriately phased polarization and magnetization with $\vec{M} = -2\vec{H}$ and $\vec{P} = -2\epsilon_0\vec{E}$. Note that using the geometry of Fig. 7(a), the E field only has a tangential component whereas the H field has both a tangential and a normal component. We therefore have $\vec{E}_2 = \vec{E}_1$, and also $\vec{H}_{t2} = \vec{H}_{t1}$. The requirement that $\vec{B}_{n2} = \vec{B}_{n1}$ further implies that $\vec{H}_{n2} + \vec{M}_n = \vec{H}_{n1}$, which with the assumed magnetization

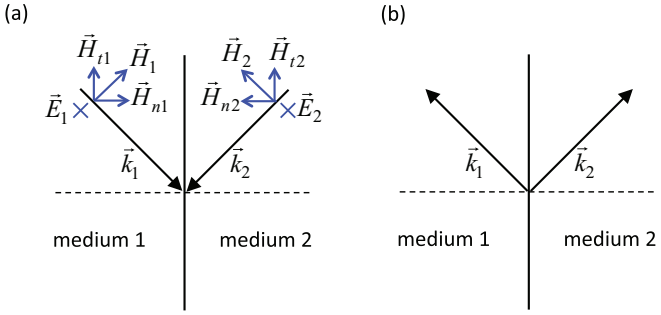

FIG. 7. (Color online) (a) Beam refraction from a "normal," right-handed material into a material with induced polarization and magnetization. The wave refracts with a negative angle of refraction. (b) The time-reversed case where the wave refracts from the material with induced polarization and magnetization into right-handed material.

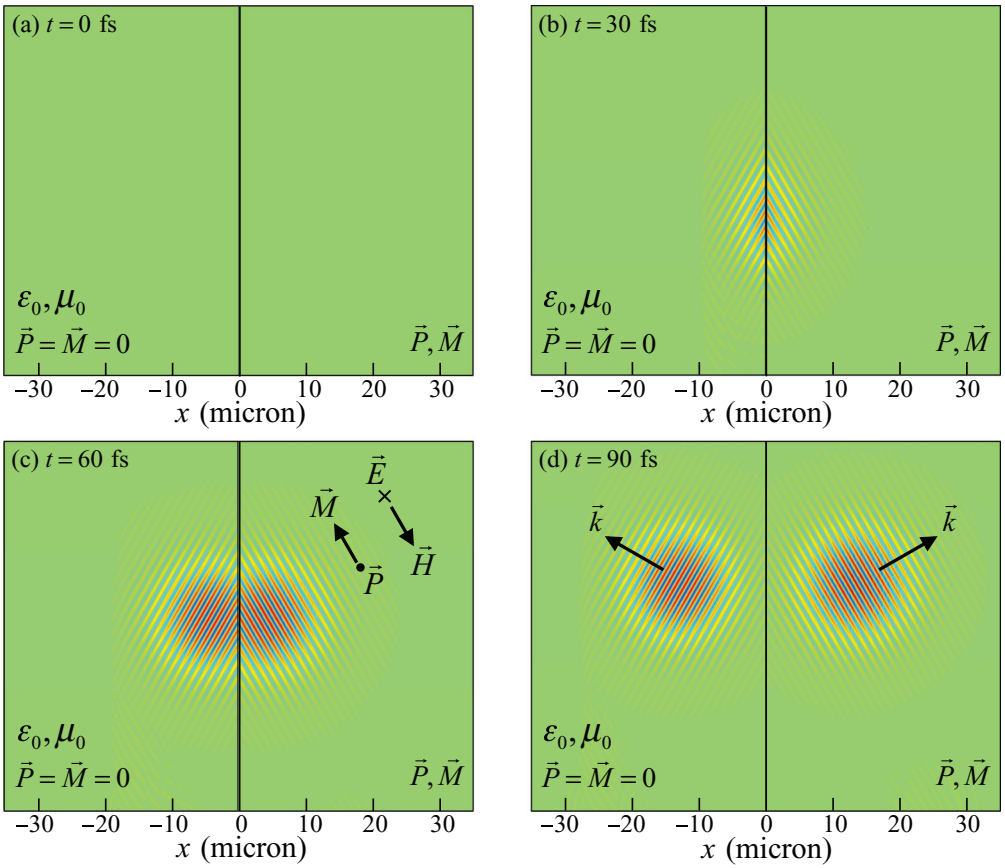

FIG. 8. (Color online) Wave refraction from a material with induced polarization and magnetization into free space. Here, we assume polarization and magnetization waves in the material propagating along the k vector as shown in Fig. 4(b) and start with zero initial field values, $\mathcal{E}_z(x,y,t=0) = \mathcal{H}_y(x,y,t=0) = 0$. Before the polarization and magnetization exist in the region on the right, there is no generated EM wave (a). Once the induced polarization and magnetization appear at the interface, a refracted right-handed wave appears in the region of free space (b). As the polarization and magnetization generate the left-handed wave in the region of $x > 0$ a refracted wave is generated along with it in the region of free space. The direction of the polarization, magnetization, electric field, and magnetic field are indicated (c). After the pulse of polarization and magnetization has completely entered the region of $x > 0$ the left-handed wave inside the material and the refracted right-handed wave outside the material become two separate pulses and propagate as expected (d).

yields $\vec{H}_{n2} = -\vec{H}_{n1}$. From these considerations, we conclude that the beam will refract at the interface with a negative angle, with the k vectors as shown in Fig. 7(a). Note that this analysis is very similar to Veselago's original analysis of wave refraction into a negative-index material [1]. Figure 7(b) shows the time-reversed case where the wave refracts from the material with induced polarization and magnetization into free space.

In Fig. 8, we numerically simulate refraction of a wave from the material with induced polarization and magnetization into free space [i.e., for the conditions of Fig. 7(b)]. Here, we assume polarization and magnetization waves in the material propagating along the k vector as shown in Fig. 7(b), away from the interface. Similar to the numerical simulation of Fig. 6, we start with zero initial field values, $\mathcal{E}_z(x,y,t=0) = \mathcal{H}_y(x,y,t=0) = 0$. The induced polarization and magnetization generates the left-handed wave in the material, which in turn refracts into free space. The false-color plots in Fig. 8 show the snapshots for the electric field $\mathcal{E}_z$ in the two spatial dimensions, x and y, at $t = 0$, $t = 30$, $t = 60$, and $t = 90$ fs. The boundary between the two regions is at $x = 0$. The region $x < 0$ is free space and the region $x > 0$ is the material with induced polarization and magnetization. As expected, the wave refracts into free space with a negative angle of refraction.

VI. IMPLEMENTATION USING A RARE-EARTH-DOPED CRYSTAL

Rare-earth ions in doped crystals at cryogenic temperatures offer a promising route for the studies of left-handed electromagnetic waves in atomic systems. The chief difficulty for observing these effects in the optical region of the spectrum is the weakness of the magnetic response. Although externally polarizing a sample is relatively straightforward, producing substantial magnetization requires a strong magnetic-dipole transition with a narrow linewidth, which is challenging to achieve. This challenge can be overcome using the intraconfigurational $4f \rightarrow 4f$ transitions of rare-earth ions [29–34]. Rare earths typically form trivalent ions in crystals with only $4f$ electrons remaining in the outer shell in the ground configuration. The $4f$ shell is tightly bound to the nucleus and the $4f$ electronic configuration interacts weakly with the crystal environment. As a result, the intraconfigurational $4f \rightarrow 4f$ transitions are sharp, and they are very much like

free-ion transitions that are only weakly perturbed by the crystal field. At cryogenic temperatures, homogeneous linewidths well below 1 MHz are routinely observed for the $4f \rightarrow 4f$ transitions [29,35,36]. Optically excited fluorescence level lifetimes exceeding 1 ms have also been demonstrated in these systems. Furthermore, due to the absence of atomic motion, there is neither Doppler broadening nor atomic diffusion. Because of these properties, rare-earth-doped crystals more closely resemble ultracold clouds than warm vapors.

Another attractive feature of these systems is that doping fractions of ~0.1% are routinely used, which corresponds to rare-earth ion densities exceeding $10^{19}/\text{cm}^3$. These densities are much higher than what can be achieved in neutral ultracold clouds or atomic vapors. The rare-earth ion-ion interactions do not significantly effect the $4f$ configuration at these densities. However, because of the interaction with the crystal field, there is an inhomogeneous broadening of the intraconfigurational $4f \rightarrow 4f$ lines [29,35]. This broadening depends on the crystal host and the specific levels but is typically a few GHz. This broadening is unusually small for a solid-state system, which is again a result of the $4f$ configuration being relatively well shielded from the cyrstalline environment. These attractive properties have been essential in recent demonstrations of quantum interference effects such as EIT and slow light in rare-earth-doped crystals [37–42].

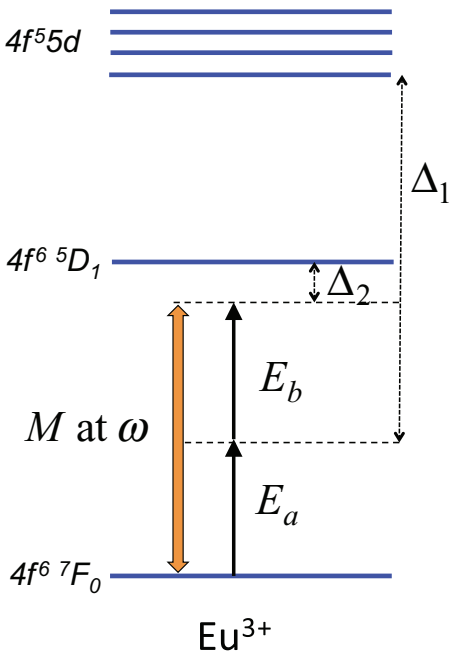

FIG. 9. (Color online) Proposed scheme for exciting left-handed waves in a Eu-doped crystal. The magnetization (M) is induced using the $^7F_0 \rightarrow {}^5D_1$ strong magnetic-dipole transition of the Eu^{3+} ions. Two-photon excitation with infrared light at a wavelength of 1054 nm is used to generate the coherence between the two levels. The two-photon excitation is through the $4f5d$ configuration as the intermediate level. The polarization can be induced using a number of processes. One approach would be to use the second-order nonlinear response of the host crystal. The second-order susceptibility ($\chi^{(2)}$) of the crystal can produce a nonlinear polarization $P = \epsilon_0 \chi^{(2)} E_c^2$ using a separate infrared laser with field amplitude E_c.

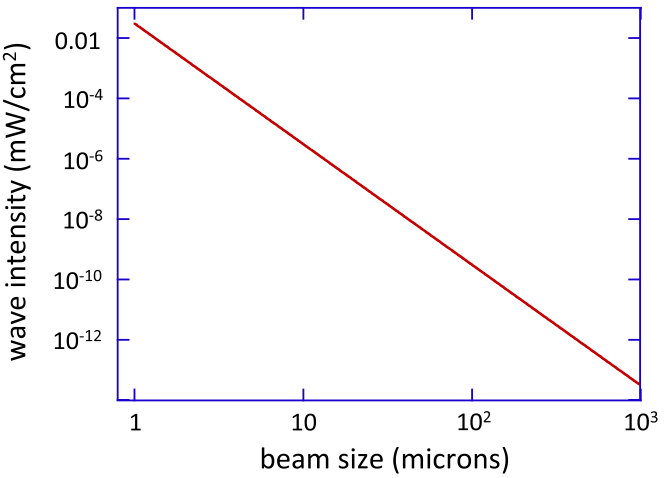

FIG. 10. (Color online) The predicted intensity of left-handed waves that can be excited inside a 0.1% doped Eu:YSO crystal. Here we take the power of the infrared laser beam ($\lambda = 1054$ nm) to be 1 W and calculate the magnetization that can be induced in the material as we vary the focused beam size. The induced magnetization in turn determines the field values and therefore the intensity for the left-handed waves.

We have identified europium (Eu)–doped crystals to be particularly suitable for the studies of left-handed waves [43]. One of the main reasons is that we have found a strong magnetic-dipole transition from the ground level in Eu^{3+}, $^7F_0 \rightarrow {}^5D_1$ transition in the $4f$ shell at an experimentally accessible wavelength of 527 nm. Figure 9 shows a specific scheme that can be used to magnetize the crystal. To generate the coherence between the two levels, two-photon excitation with an intense beam of infrared light at a wavelength of 1054 nm can be used. The transitions within the $4f$ shell in a free ion are dipole forbidden due to parity selection rules (inside the crystal, these transitions become weakly dipole allowed due to the mixing with the crystal field; however, this mixing is small). However, a two-photon excitation using the high-lying $4f5d$ configuration as an intermediate level can be used [44–47]. The goal would be to produce a reasonably large coherence of the magnetic dipole transition, ρ_{gm}, and therefore produce a substantial magnetization at the doubled frequency. To find the magnetic-dipole matrix element between the $^7F_0$ and $^5D_1$ levels of the $4f$ shell, we used Cowan's atomic structure code [48]. Cowan's code gives the magnetic-dipole decay rate (Einstein A coefficient) from the excited level $^5D_1$ to $^7F_0$ to be 7.1 s^{-1}. We have found two references that have either experimentally measured or numerically calculated this decay rate. They specify this decay rate to be 10.3 s^{-1} [49] and 10.8 s^{-1} [50], respectively, which is in reasonable agreement with our calculation using Cowan's code. Based on the decay rate, we calculate the magnetic-dipole matrix element for the $^7F_0 \rightarrow {}^5D_1$ transition to be $\mu_{gm} \equiv \langle J||\hat{\mu}||J'\rangle \approx 0.1\mu_B$, which is reasonably strong.

Figure 10 shows the calculated intensity of left-handed waves that can be excited in a Eu-doped crystal with experimental parameters that can be achieved relatively easily. Here we assume a 0.1% doped crystal and take the power of the 1054-nm infrared beam to be 1 W. For a given focused spot size

of the infrared beam, we calculate the induced magnetization using the following procedure. We first calculate the Rabi frequency for each step in the two-photon excitation, which is proportional to the product of the electric field and the dipole matrix element between the $4f$ and $4f5d$ configurations. We then calculate the established coherence of the magnetic-dipole transition using Eq. (7) with $\Delta_1 = 50\,000$ cm^{-1} (which is the large detuning from the $4f5d$ configuration) and $\Delta_2 =$ 1.5 GHz (which is the inhomogeneous linewidth of the transition). With the established coherence calculated, we calculate the induced magnetization in the crystal using Eq. (6). The induced magnetization in turn determines the field values for the left-handed waves (using $|\vec{H}| = |\vec{M}|/2$). Figure 10 shows the calculated intensity of the left-handed waves as the focused spot size of the 1054-nm beam is varied. Even for a reasonably large spot size of 100 μm, it should be possible to excite left-handed waves with easily detectible intensity levels.

A quick calculation reveals that inducing polarization in the crystal should be relatively straightforward. One idea would, for example, be to use the second-order nonlinearity of the host crystal. Due to the second-order susceptibility, $\chi^{(2)}$, a separate infrared field E_c will produce a nonlinear polarization of magnitude $P = \epsilon_0 \chi^{(2)} E_c^2$. Even if we assume a second-order susceptibility which is many orders of magnitude smaller than other common crystals [for example, quartz (SiO_2) and many other crystals have $\chi^{(2)} \approx 10^{-12}$ m/V], we calculate that it is not difficult to induce a sufficiently large polarization in the crystal as required for left-handed wave generation of Fig. 10.

VII. CONCLUSIONS

In conclusion, we have discussed left-handed waves in materials where the medium is polarized and magnetized externally, i.e., by processes that do not depend on the incident wave. Compared to materials with a negative refractive index, there is one clear advantage of materials with induced polarization and magnetization: The formation of left-handed waves does not require the stringent material properties. We have presented analytical results as well as numerical simulations that show left-handed wave propagation and negative refraction at an interface. We have also discussed a realistic approach to generating left-handed waves in a rare-earth-doped crystal. Left-handed electromagnetic waves manifest a lot of exciting physics and have the potential for a number of practical applications. Over the past decade, negative-index materials have generated a lot of enthusiasm. It is now well understood that these materials have important practical applications such as constructing "perfect lenses" that can, in principle, image objects with arbitrarily high resolution. Materials with induced polarization and magnetization appear to share much of the physics of negative-index materials. Perhaps many of the applications of materials with induced polarization and magnetization will be revealed by exploring the exact correspondence between these materials and negative-index materials. However, we note that because materials with induced polarization and magnetization appear to have unique properties (such as the direction of the group velocity), they deserve a careful study on their own.

ACKNOWLEDGMENTS

We acknowledge many helpful discussions with Zach Simmons, Josh Weber, and Jared Miles. This work was supported by the Air Force Office of Scientific Research (AFOSR).

[1] V. G. Veselago, Sov. Phys. Usp. **10**, 509 (1968).
[2] J. B. Pendry, Phys. Rev. Lett. **85**, 3966 (2000).
[3] D. R. Smith and N. Kroll, Phys. Rev. Lett. **85**, 2933 (2000).
[4] S. Foteinopoulou, E. N. Economou, and C. M. Soukoulis, Phys. Rev. Lett. **90**, 107402 (2003).
[5] D. Schurig, J. J. Mock, B. J. Justice, S. A. Cummer, J. B. Pendry, A. F. Starr, and D. R. Smith, Science **314**, 977 (2006).
[6] J. Valentine, J. Li, T. Zentgraf, G. Bartal, and X. Zhang, Nat. Mater. **8**, 568 (2009).
[7] R. A. Shelby, D. R. Smith, and S. Shultz, Science **292**, 77 (2001).
[8] A. A. Houck, J. B. Brock, and I. L. Chuang, Phys. Rev. Lett. **90**, 137401 (2003).
[9] P. V. Parimi, W. T. Lu, P. Vodo, J. Sokoloff, J. S. Derov, and S. Sridhar, Phys. Rev. Lett. **92**, 127401 (2004).
[10] E. Cubukcu, K. Aydin, E. Ozbay, S. Foteinopoulou, and C. M. Soukoulis, Nature (London) **423**, 604 (2003).
[11] T. J. Yen, W. J. Padilla, N. Fang, D. C. Vier, D. R. Smith, J. B. Pendry, D. N. Basov, and X. Zhang, Science **303**, 1494 (2004).
[12] V. M. Shalaev, W. Cai, U. K. Chettiar, H. Yuan, A. K. Sarychev, V. P. Drachev, and A. V. Kildishev, Opt. Lett. **30**, 3356 (2005).
[13] S. Zhang, W. Fan, N. C. Panoiu, K. J. Malloy, R. M. Osgood, and S. R. J. Brueck, Phys. Rev. Lett. **95**, 137404 (2005).
[14] G. Dolling, C. Enkrich, M. Wegener, C. M. Soukoulis, and S. Linden, Opt. Lett. **31**, 1800 (2006).
[15] M. S. Rill, C. Plet, M. Thiel, I. Staude, G. Freymann, S. Linden, and M. Wegener, Nat. Mater. **7**, 543 (2008).
[16] H. J. Lezec, J. A. Dionne, and H. A. Atwater, Science **316**, 430 (2007).
[17] M. Ö. Oktel and Ö. E. Müstecaplioğlu, Phys. Rev. A **70**, 053806 (2004).
[18] Q. Thommen and P. Mandel, Phys. Rev. Lett. **96**, 053601 (2006).
[19] J. Kästel, M. Fleischhauer, S. F. Yelin, and R. L. Walsworth, Phys. Rev. Lett. **99**, 073602 (2007).
[20] J. Kästel, M. Fleischhauer, S. F. Yelin, and R. L. Walsworth, Phys. Rev. A **79**, 063818 (2009).
[21] D. E. Sikes and D. D. Yavuz, Phys. Rev. A **82**, 011806(R) (2010).
[22] D. E. Sikes and D. D. Yavuz, Phys. Rev. A **84**, 053836 (2011).
[23] P. P. Orth, R. Hennig, C. H. Keitel, and J. Evers, New J. Phys. **15**, 013027 (2013).
[24] M. O. Scully and M. S. Zubairy, *Quantum Optics* (Cambridge University Press, Cambridge, UK, 1997).
[25] S. E. Harris, Phys. Today **50**(7), 36 (1997).
[26] A. D. Boardman, V. V. Grimalsky, Y. S. Kivshar, S. V. Koshevaya, M. Lapine, N. M. Litchinitser, V. N. Malnev, M. Noginov, Y. G. Rapoport, and V. M. Shalaev, Lasers Photonics Rev. **5**, 287 (2011).

[27] S. Xiao, V. P. Drachev, A. V. Kildishev, N. Xingjie, U. K. Chettiar, Y. Hsiao-Kuan, and V. M. Shalaev, Nature (London) **466**, 735 (2010).
[28] K. S. Yee, IEEE Trans. Antennas Propagat. **AP-14**, 302 (1966).
[29] R. M. Macfarlane, J. Lumin. **100**, 1 (2002).
[30] B. G. Wybourne, *Spectroscopic Properties of Rare-Earths* (John Wiley & Sons, New York, 1965).
[31] K. N. R. Taylor and M. I. Darby, *Physics of Rare Earth Solids* (Chapman and Hall, London, 1972).
[32] G. S. Ofelt, J. Chem. Phys. **38**, 2171 (1963).
[33] G. S. Ofelt, J. Chem. Phys. **37**, 511 (1962).
[34] G. H. Dieke and H. M. Crosswhite, Appl. Optics **2**, 675 (1963).
[35] R. M. Macfarlane and R. M. Shelby, J. Lumin. **36**, 179 (1987).
[36] R. W. Equall, Y. Sun, R. L. Cone, and R. M. Macfarlane, Phys. Rev. Lett. **72**, 2179 (1994).
[37] B. S. Ham, P. R. Hemmer, and M. S. Shahriar, Opt. Commun. **144**, 227 (1997).
[38] B. S. Ham, P. R. Hemmer, and M. S. Shahriar, Phys. Rev. A **59**, R2583(R) (1999).
[39] A. V. Turukhin, V. S. Sudarshanam, M. S. Shahriar, J. A. Musser, B. S. Ham, and P. R. Hemmer, Phys. Rev. Lett. **88**, 023602 (2001).
[40] J. Klein, F. Beil, and T. Halfmann, J. Phys. B: At. Mol. Opt. Phys. **40**, S345 (2007).
[41] J. Klein, F. Beil, and T. Halfmann, Phys. Rev. Lett. **99**, 113003 (2007).
[42] J. Klein, F. Beil, and T. Halfmann, Phys. Rev. A **78**, 033416 (2008).
[43] B. Lauritzen, N. Timoney, N. Gisin, M. Afzelius, H. de Riedmatten, Y. Sun, R. M. Macfarlane, and R. L. Cone, Phys. Rev. B **85**, 115111 (2012).
[44] R. T. Wegh and A. Meijerink, Phys. Rev. B **60**, 10820 (1999).
[45] L. van Pieterson, M. F. Reid, G. W. Burdick, and A. Meijerink, Phys. Rev. B **65**, 045114 (2002).
[46] L. van Pieterson, M. F. Reid, R. T. Wegh, S. Soverna, and A. Meijerink, Phys. Rev. B **65**, 045113 (2002).
[47] L. van Pieterson, M. F. Reid, and A. Meijerink, Phys. Rev. Lett. **88**, 067405 (2002).
[48] R. D. Cowan, *The Theory of Atomic Structure and Spectra* (University of California Press, Oakland, 1981).
[49] M. J. Weber and R. F. Schaufele, J. Chem. Phys. **43**, 1702 (1965).
[50] W. F. Krupke, Phys. Rev. **145**, 325 (1966).